Effect of spurious reflection on phase shift interferometry

Chiayu Ai and James C. Wyant

The phase errors caused by spurious reflection in Twyman-Green and Fizeau interferometers are studied. A practical algorithm effectively eliminating the error is presented. Two other algorithms are reviewed, and the results obtained using the three algorithms are compared.

I. Introduction

In the presence of spurious reflection, there are more than two beams interfering. The influence of extraneous light on the accuracy of phase measurement has been discussed briefly by Bruning[1] and in detail by Schwider *et al.*[2] for simplified extraneous interference. In real life extraneous interference is complex and is always a troublesome problem, especially when high accuracy is required. In this paper, this problem is studied in detail, and a vector representation is used for conciseness.

For an extraneous beam of light with a constant phase over the pupil, the error has a frequency equal to the spatial frequency of the interference fringe, unlike the errors caused by piezoelectric transducer linear calibration and nonlinearity, or by vibration.[3–5] Therefore, averaging two runs of phase measurement with a 90° phase shift relative to each other cannot remove the error caused by spurious reflection. A method requiring an additional phase shifter in the test arm was suggested by Schwider *et al.* to reduce the error. In this paper a practical method is presented for reducing the error without the additional phase shifter. The results using the simple arctangent formula, Schwider's algorithm, and this proposed method are presented.

The error for a multiple-reflection situation is studied. If the reflectivities of the test and reference surfaces are about the same, the extra reflection of the test beam from the reference surface has a second-order effect on phase error. But if the test surface has a high reflectivity, the error will be complex. The scattering or reflection from the optics in the image arm is studied also.

II. Theory

An ideal interferometer has only two beams of light interfering; one is from the test arm and the other from the reference arm. In reality, however, more than two beams interfere because of some spurious reflections. These extraneous beams and the test and reference beams may interfere coherently because of the enormous coherence length of laser light. For example, in a Fizeau-type interferometer, the reference surface will reflect part of the test beam back into the test arm and hence cause extraneous interference. In both Twyman-Green and Fizeau interferometers, the rear surface of the beam splitter and the surfaces of the divergent lens can introduce some spurious reflections, and thus extraneous interference appears if these surfaces are not coated properly. Even scattered light from all the surfaces contributes to extraneous interference. In most situations, this scattered light is too dim in intensity to affect the measurement, and the interference fringes caused by it are too dense to detect. However, scattering from the imaging lens causes significant error, especially when there is some defect or improper coating on the imaging lens. The scattering source is so close to the detector that the intensity of this scattering is no longer negligible. Thus an error in the phase measurement occurs.

To establish the notation, we first briefly review the work done by Schwider *et al.*[2] In the presence of extraneous coherent light, the intensity distribution is no longer of the two-beam interference type. Let us assume that there is one extra beam from the test arm and/or the reference arm but that it is not reflected from the test surface or the reference surface. Then the complex amplitudes of the three beams can be written as

The authors are with University of Arizona, Optical Sciences Center, Tucson, Arizona 85721.

Received 15 January 1988.
0003-6935/88/143039-07$02.00/0.

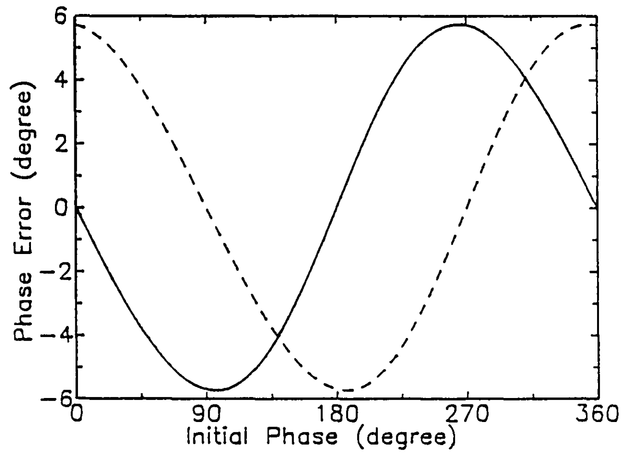

Fig. 1. Phase error due to the extraneous beam. For a given Θ, the error is a function of the phase Φ and has a frequency equal to the spatial frequency of the interference fringe. The solid curve is for Θ = 0°, and the dashed curve is for Θ = 90°

$A_t \cdot \exp(i\phi_t)$ from the test arm without extraneous beam,
$A_r \cdot \exp(i\phi_r)$ from reference arm without extraneous beam,
$E \cdot \exp(i\eta)$ from extraneous beam,

where A_t, A_r, E, ϕ_t, ϕ_r, and η are the amplitudes and phases of the three beams, respectively. The three-beam interference intensity is

$$I = A_t^2 + A_r^2 + E^2 + 2A_t \cdot E \cdot \cos(\phi_t - \eta) + 2A_t \cdot A_r \cdot \cos(\phi_t - \phi_r) + 2A_r \cdot E \cdot \cos(\eta - \phi_r). \quad (1)$$

The first four terms do not vary while the reference surface is shifting. Therefore, by shifting the reference phase 90° between each step, the intensities of the four steps are

$$I_n = \text{constant} + 2A_t \cdot A_r \cdot \cos(\phi_t - \phi_r - n \cdot 90°) + 2A_r \cdot E \cdot \cos(\eta - \phi_r - n \cdot 90°), \quad (2)$$

where n = 0, 1, 2, and 3. If the simple arctangent formula[6]

$$\phi_t - \phi_r = \tan^{-1}\frac{I_3 - I_1}{I_0 - I_2} \quad (3)$$

is used to calculate the phase Φ, the resulting phase ϕ' and the error $(\Phi' - \Phi)$ are given as

$$\Phi' = \tan^{-1}\frac{A_t \cdot \sin(\Phi) + E \cdot \sin(\Theta)}{A_t \cdot \cos(\Phi) + E \cdot \cos(\Theta)}, \quad (4)$$

$$\Phi' - \Phi = \tan^{-1}\left[\frac{E \cdot \sin(\Theta - \Phi)}{A_t + E \cdot \cos(\Theta - \Phi)}\right], \quad (5)$$

where $\Phi \equiv \phi_t - \phi_r$ and $\Theta \equiv \eta - \phi_r$. Equations (4) and (5) were first derived by Schwider *et al.*[2] and Bruning,[1] respectively. The error is a function of Θ and Φ. From Eq. (5), it is the ratio of E to A_t and the difference between Θ and Φ that determine the phase error. For a given A_t and E, the maximum error occurs when the derivative of $\Phi' - \Phi$ in Eq. (5) with respect to $\Theta - \Phi$ is equal to zero, i.e.,

$$A_t \cdot |\cos(\Theta - \Phi)| - E = A_t \cdot |\cos(\eta - \phi_t)| - E = 0. \quad (6)$$

From Eq. (5), for a given Θ, the error is a function of Φ and has a frequency equal to the spatial frequency of the interference fringe, as shown in Fig. 1. Likewise, for a given Φ the phase error has a similar result. If the phase change of the extraneous beam in a direction on the image plane is much smaller than the phase change of the test beam, or vice versa, this single spatial frequency error occurs along that direction. For a general case, the phases of both the extraneous and test beams vary on the image plane. Let us assume that the phases of the test and the extraneous beams, relative to ϕ_r along the x direction are like tilts, given as

$$\Phi(x) = \phi_{t0} + 2\pi \cdot f_t \cdot x - \phi_r, \quad (7)$$

$$\Theta(x) = \eta_0 \pm 2\pi \cdot f_e \cdot x - \phi_r, \quad (8)$$

where f_t and f_e are the corresponding spatial frequencies. Therefore, the phase error obtained using Eq. (3) has a spatial frequency of either $f_t - f_e$ or $f_t + f_e$, depending on the sign in Eq. (8) being plus or minus.

These errors are unlike the errors caused by piezoelectric transducer linear calibration and nonlinearity, or by vibration,[3–5] which have a double spatial frequency error and can be reduced by averaging two runs of phase measurements, with a 90° phase shift relative to each other. However, because the error caused by the extraneous beam does not change while the reference mirror is moved in the second run, averaging two runs of phase measurement cannot reduce this error.

III. Algorithms

An algorithm has been suggested by Schwider *et al.*[2] to eliminate completely the error introduced by the extraneous beam. In this algorithm, an additional phase shifter is added in the test arm to introduce a 180° phase shift for the test beam, then an additional four frame intensities I'_0, I'_1, I'_2, and I'_3 are taken. Thus the phase Φ is obtained using

$$\Phi = \tan^{-1}\frac{(I_1 - I_3) - (I'_1 - I'_3)}{(I_0 - I_2) - (I'_0 - I'_2)}. \quad (9)$$

Since the intensities of Eq. (2) are trigonometric functions, it is convenient to represent them by phasors. Let

$$\mathcal{P} \equiv 4A_t \cdot A_r \cdot \exp i(\phi_t - \phi_r), \quad (10)$$

$$\mathcal{E} \equiv 4A_r \cdot E \cdot \exp i(\eta - \phi_r). \quad (11)$$

Then from Eq. (1)

$$I_0 = A_t^2 + A_r^2 + E^2 + 2A_t \cdot E \cdot \cos(\eta - \phi_t) + \mathrm{Re}[0.5 \cdot (\mathcal{P} + \mathcal{E})], \quad (12)$$

and similar expressions are obtained for I_1, I_2, and I_3; hence

$$I_1 - I_3 = \mathrm{Im}(\mathcal{P} + \mathcal{E}), \quad (13)$$

$$I_0 - I_2 = \mathrm{Re}(\mathcal{P} + \mathcal{E}), \quad (14)$$

Therefore, the phase of the sum of $\mathcal{P}$ and $\mathcal{E}$ determines the resulting phase Φ′, as shown in Fig. 2. From this figure, it can be seen that the resulting phase has a

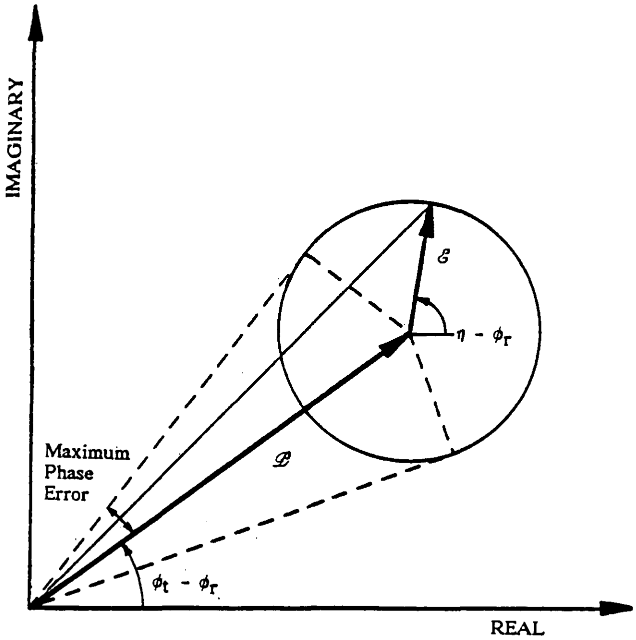

Fig. 2. Schematic of the relation of the resulting phase error to the test beam and the extraneous beam. The maximum error occurs when the phasor $\mathcal{E}$ is perpendicular to the sum of $\mathcal{P}$ and $\mathcal{E}$.

maximum error equal to the arccosine of the ratio of $|\mathcal{E}|$ to $|\mathcal{P}|$, when the phasor $\mathcal{E}$ is perpendicular to the sum of $\mathcal{P}$ and $\mathcal{E}$, as depicted in Eq. (6).

Using vector representation, a 180° phase shift for the test beam results in the sign change of $\mathcal{P}$. Therefore,

$$(I_1' - I_3') = \mathrm{Im}[-\mathcal{P} + \mathcal{E}], \tag{15}$$

$$(I_1 - I_3) - (I_1' - I_3') = \mathrm{Im}[(\mathcal{P} + \mathcal{E}) - (-\mathcal{P} + \mathcal{E})]. \tag{16}$$

Similarly,

$$(I_0 - I_2) - (I_0' - I_2') = \mathrm{Re}[(\mathcal{P} + \mathcal{E}) - (-\mathcal{P} + \mathcal{E})]. \tag{17}$$

Thus $\mathcal{E}$ is totally removed from the numerator and the denominator of Eq. (9), and the error is completely eliminated.

Actually, to remove $\mathcal{E}$ from the sum of $\mathcal{P}$ and $\mathcal{E}$, we can simply block the beam from the test surface, take four additional intensities, I_0', I_1', I_2', I_3', and subtract them from I_0, I_1, I_2, and I_3. Therefore,

$$(I_0 - I_2) - (I_0' - I_2') = \mathrm{Re}[(\mathcal{P} + \mathcal{E}) - (\mathcal{E})], \tag{18}$$

$$(I_1 - I_3) - (I_1' - I_3') = \mathrm{Im}[(\mathcal{P} + \mathcal{E}) - (\mathcal{E})]. \tag{19}$$

Thus the error is removed, and the phase Φ is obtained using Eq. (9). It should be noted that I_i' here is the intensity after the test beam is blocked, and I_i' in Schwider's algorithm is the intensity after the test beam is shifted 180° in phase.

IV. Experimental Results

A wedge is inserted in the test arm of a Twyman-Green interferometer to introduce spurious reflection. Figure 3(a) is the intensity distribution for three-beam interference. The two-beam interference of the refer-

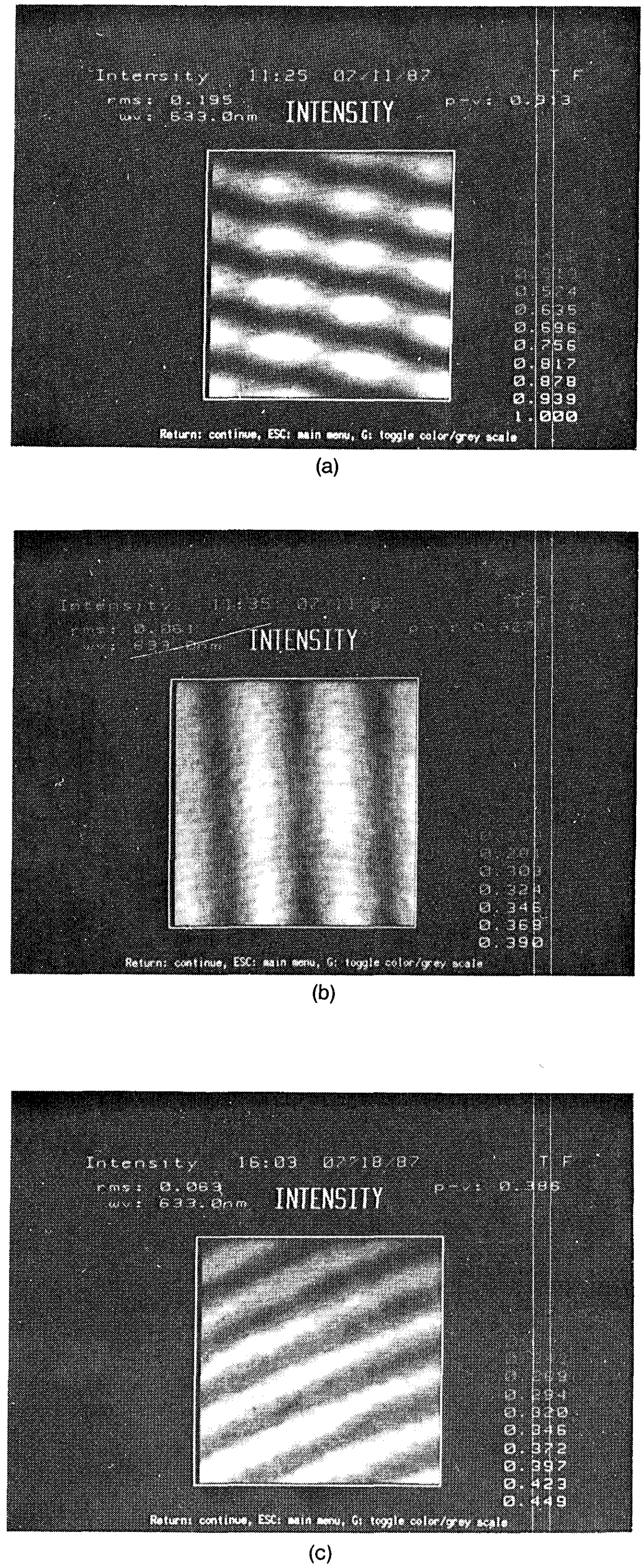

Fig. 3. (a) Three-beam interference of the test, reference, and extraneous beams. (b) Two-beam interference of the reference and extraneous beams. (c) Two-beam interference of the test and extraneous beams. The vertical fringes in (a) are due to the spurious reflection.

ence and extraneous beams, for which the fringes are vertical, is shown in Fig. 3(b). The interference of the test and the extraneous beams is illustrated in Fig. 3(c). The very fine and faint horizontal fringes are due to the reflection or scattering in the image arm. The amplitude of this reflection or scattering is so small that the error caused by it is not noticeable.

The three resulting phases, obtained using the simple algorithm, Schwider's algorithm, and the new algorithm, are presented in Fig. 4, respectively. The rms values of the phase, obtained using the three algorithms, are 0.020λ, 0.006λ, and 0.006λ, respectively, where 0.006λ mainly is due to the surface roughness. The difference between 0.020λ and 0.006λ is the error caused by spurious reflection. The cross sections of the resulting phases of Fig. 4 are illustrated in Fig. 5.

The rms of the phase obtained by averaging two runs of phase measurement, with a 90° phase shift relative to each other, is 0.020λ, and the corresponding phase map is the same as that in Fig. 4(a). Therefore, averaging two runs of phase measurement cannot remove the error caused by spurious reflection. In Fig. 4(c), there are residual errors that could be caused by the phase shift introduced in the test arm being not exactly at 180°.

The resulting phase in Fig. 4(a) has a similar pattern as the interference intensity distribution in Fig. 3(a). But the orientation of the resulting phase in Fig. 4(a) is different from that in Fig. 3(a). The difference is due to the moire fringe effect. Comparing Figs. 4(a) and 3(c), the phase error has a pattern similar to the intensity distribution of the interference of the test and extraneous beams. This can be explained as follows. The phases of the test and the extraneous beams do not change while the reference phase is varying. The composition of the test and extraneous beams determines the resulting phase and amplitude of the resulting test beam and thus determines the phase error. Thus the phase error, Fig. 4(a), has the same pattern of the phase of the resulting test beam, Fig. 3(c). Moreover, for an extraneous beam of light with a constant phase over the entire pupil, the error has a frequency equal to the spatial frequency of the interference fringe, unlike the errors caused by the piezoelectric transducer linear calibration and nonlinearity or by vibration.[3–5]

V. Multiple Reflection

In the above, we assume that the extraneous beam is reflected from the test arm and/or the reference arm but is not reflected from the test surface or the reference surface. For example, in the test arm of a Twyman-Green interferometer, the collimating beam through the beam splitter reflected from the diverging lens is in this category. For this type of spurious beam, the algorithm proposed can completely remove the phase error caused by it.

It should be noted that if the extra beams have been reflected by the reference surface or by the test surface, such as the beam first reflected from the test surface and then reflected from the diverger back to the test surface, the proposed algorithm does not apply. For

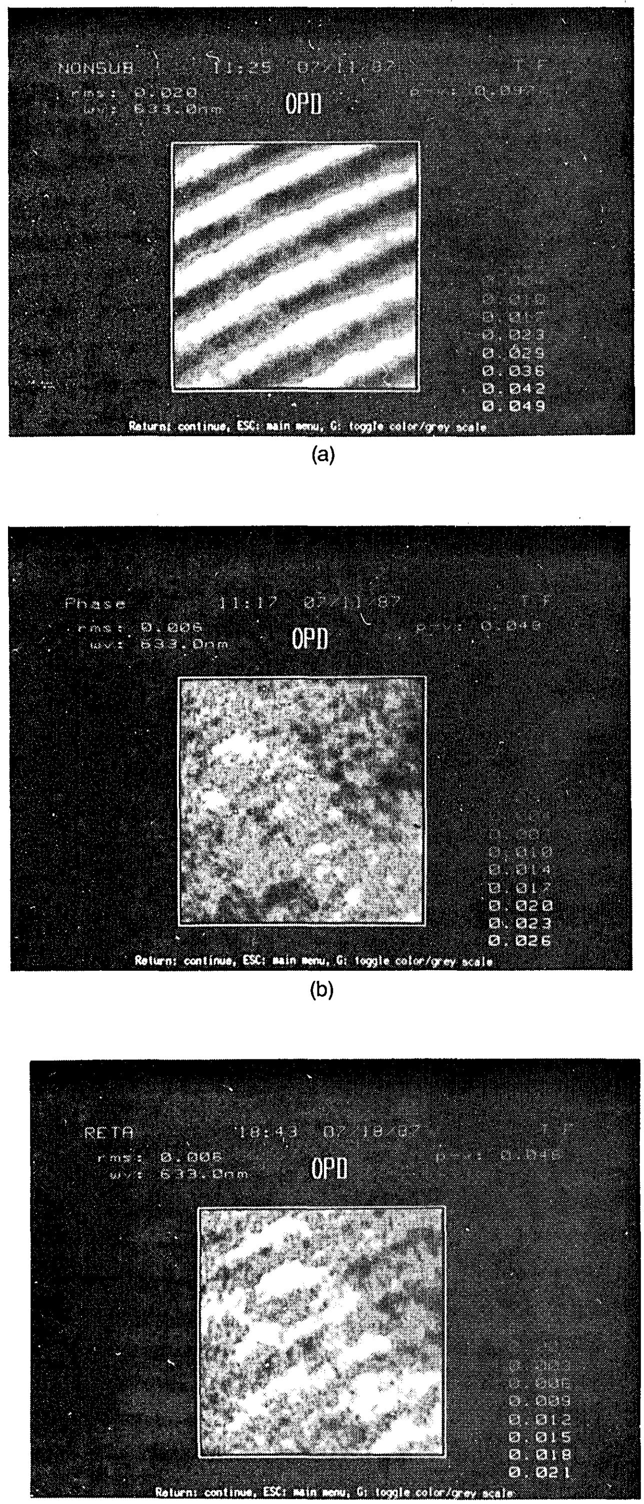

Fig. 4. Resulting phase of three-beam interference obtained using (a) the simple arctangent formula, (b) the new algorithm, and (c) Schwider's algorithm. It should be noted that the phase error of (a) has the same pattern as the intensity distribution in Fig. 3(c).

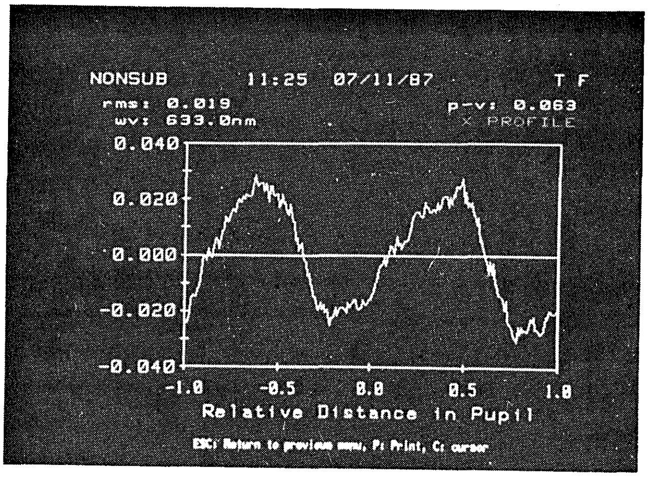

(a)

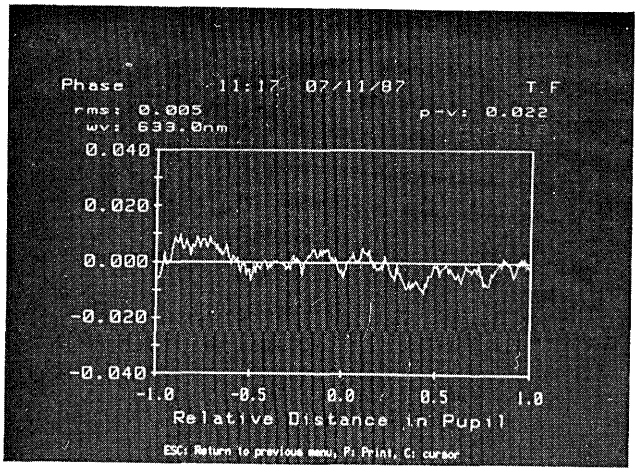

(b)

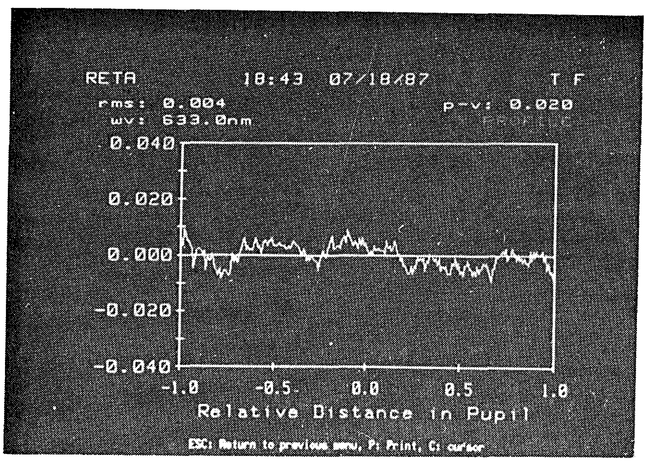

(c)

Fig. 5. Cross sections of the resulting phases of Fig. 4. (a), (b), and (c) are the cross sections of Figs. 4(a), (b), and (c), respectively.

this case, the phase of the extra beam in the reference arm varies synchronously with the phase shifting of the reference mirror, and the extra beam in the test arm has a fixed phase difference from the true test beam. Therefore, this type of extra beam cannot be extracted out.

The extraneous beams due to the reflection of the rear surface of the beam splitter fall into this category. Therefore, for a beam splitter, not only the surface figure is critical to the measurement but the antireflection coating of the rear surface. For some Fizeau interferometers the reflection from the rear surface of the beam splitter is also an error source, if there is a beam splitter. Using a wedged beam splitter is a simple solution to this problem.

For a Fizeau interferometer, the reference surface inevitably reflects part of the test beam back into the test arm and hence causes extraneous interference, for which the above algorithm does not apply. In the following, we discuss the effect of the extra reflection of the test beam from the reference surface. When the reference surface reflects part of the test beam back into the test arm, there is multiple-beam interference. The complex amplitudes of the multiple beams can be written as

$$\mathcal{R} \equiv r \cdot \exp(i\phi_r) \qquad \text{from reference arm,}$$

$$\mathcal{T} \equiv r_t \cdot \exp(i\phi_t) \qquad \text{from test arm without extraneous beam,}$$

$$\mathcal{E} \equiv \mathcal{T} \cdot \mathcal{R}^* \cdot \mathcal{T}' \cdot \{1 + \mathcal{R}^* \cdot \mathcal{T}'' \cdot [1 + \mathcal{R}^* \cdot \mathcal{T}''' \cdot (1 + \ldots)]\} \qquad \text{from extraneous beam,}$$

where r and r_t are the reflectivities of the reference and test surfaces, respectively. $\mathcal{R}^*$ is the complex conjugate of $\mathcal{R}$ due to the rear reflection of the reference surface, and $\mathcal{T}'$, $\mathcal{T}''$, $\mathcal{T}'''$ are the second, third, and four reflections from the test surface. If reflectivities r and r_t are smaller than unity, the extraneous reflection approximately equals

$$\mathcal{E} \cong \mathcal{T} \cdot \mathcal{R}^* \cdot \mathcal{T}' + \mathcal{T} \cdot \mathcal{R}^* \cdot \mathcal{T}' \cdot \mathcal{R}^* \cdot \mathcal{T}'', \tag{20}$$

and the intensity is

$$I = |\mathcal{R}|^2 + |\mathcal{T}|^2 + |\mathcal{E}|^2 + \mathcal{R}^* \cdot \mathcal{T} + \mathcal{R} \cdot \mathcal{T}^* + (\mathcal{R}^* \cdot \mathcal{T} \cdot \mathcal{R}^* \cdot \mathcal{T}' + \mathcal{R}^* \cdot \mathcal{T} \cdot \mathcal{R}^* \cdot \mathcal{T}' \cdot \mathcal{R}^* \cdot \mathcal{T}'' + \text{c.c.}) + (\mathcal{T}^* \cdot \mathcal{T} \cdot \mathcal{R}^* \cdot \mathcal{T}' + \mathcal{T}^* \cdot \mathcal{T} \cdot \mathcal{R}^* \cdot \mathcal{T}' \cdot \mathcal{R}^* \cdot \mathcal{T}'' + \text{c.c.}). \tag{21}$$

The terms $\mathcal{R}^* \cdot \mathcal{T}$ and $\mathcal{R} \cdot \mathcal{T}^*$ determine the phase of interest. The first term in the first parentheses, $\mathcal{R}^* \cdot \mathcal{T} \cdot \mathcal{R}^* \cdot \mathcal{T}'$, is canceled in $I_0 - I_2$ (and $I_1 - I_3$), because $\mathcal{R}^* \cdot \mathcal{R}^*$ has a phase shift twice that of $\mathcal{R}$. Similarly, the second term in the second parentheses is canceled in $I_0 - I_2$ (and $I_1 - I_3$). The first term in the second parentheses, $\mathcal{T}^* \cdot \mathcal{T} \cdot \mathcal{R}^* \cdot \mathcal{T}'$, has a magnitude of the order of $r \cdot r_t^3$, which is the second order of $\mathcal{R}^* \cdot \mathcal{T}$, if $r \cong r_t$. Similarly, the magnitude of the second term in the first parentheses is the fourth order of $\mathcal{R}^* \cdot \mathcal{T}$ and can be ignored. Therefore, for a Fizeau interferometer, if $r \cong r_t$, the extra reflection of the test beam from the reference surface has only a second-order effect on phase error. A similar conclusion was pointed out by Hariharan.[7]

However, if the test surface has a high reflectivity, i.e., $r_t \cong 1$, the intensity including the second order r^2 is written as

$$I = \text{constant} + (\mathcal{R}^* \cdot \mathcal{T} + \text{c.c.}) + (\mathcal{T}^* \cdot \mathcal{T} \cdot \mathcal{R}^* \cdot \mathcal{T}' + \text{c.c.}) + (\mathcal{R}^* \cdot \mathcal{T} \cdot \mathcal{R}^* \cdot \mathcal{T}' + \mathcal{T}^* \cdot \mathcal{T} \cdot \mathcal{R}^* \cdot \mathcal{T}' \cdot \mathcal{R}^* \cdot \mathcal{T}'' + \text{c.c.}). \quad (22)$$

The terms in the third parentheses are canceled in $I_0 - I_2$ (and $I_1 - I_3$), because $\mathcal{R}^* \cdot \mathcal{R}^*$ has a phase shift twice that of $\mathcal{R}$. The terms in the second parentheses caused by the extraneous reflection have the same amplitude as the terms in the first parentheses. Therefore, the interference fringe patterns are very complex, and thus the phase error is much greater than that when the reflectivity of the test surface is small.

VI. Conclusion

The phase errors caused by piezoelectric transducer linear calibration and nonlinearity have a double-frequency characteristic. Averaging two runs of phase measurement, with a 90° phase shift relative to each other, has been used successfully to remove errors caused by them. However, the error caused by an extraneous beam does not change when the reference mirror is moved in the second run. Therefore, the phase error caused by it does not have such a double-frequency characteristic, and hence the averaging technique does not apply.

A practical algorithm, modified from the algorithm of Schwider *et al.*, effectively eliminates the error induced by an extraneous beam. In this algorithm, four intensities are taken as in a regular four step/bucket algorithm, then the test beam is blocked in front of the test mirror and four additional intensities are taken. By subtracting these additional four intensities from the first four intensities, the effect of the spurious reflection is removed, and thus the phase is obtained with no error. It should be noted that if the extra beams have been reflected by the reference surface or by the test surface, the proposed algorithm does not apply. For a Fizeau interferometer, if the reflectivities of the test and reference surfaces are much less than unity, the extra reflection of the test beam from the reference surface has a second-order effect on phase error. However, if the test surface is highly reflective, the interference is so complex that the phase of the test surface cannot be determined.

Appendix

In the imaging paths of both Twyman-Green and Fizeau interferometers, both the test and reference beams have a common path and hence suffer almost the same reflection/scattering from the imaging lens. Therefore, there are four beams interfering,

$B \cdot \exp[i\phi_t(x)]$	from test arm without extraneous beam,
$C \cdot \exp[i\phi_r(x)]$	from reference arm without extraneous beam,
$b \cdot \exp[i\eta_t(x)]$	from extraneous beam due to test beam,
$c \cdot \exp[i\eta_r(x)]$	from extraneous beam due to reference beam,

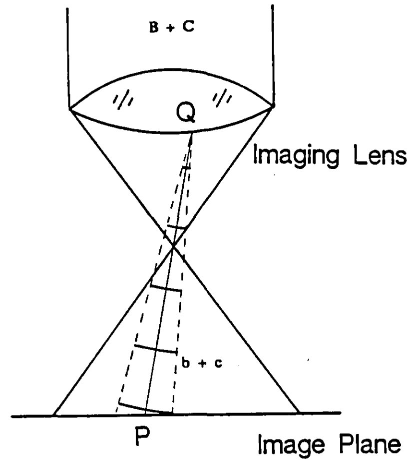

Fig. 6. Schematic of the interference due to scattered light. B and C are the test and reference beams. Their scattered beams, b and c, are from point Q on the imaging lens.

as shown in Fig. 6. For simplicity, in the following equations the variable x is dropped. Using Babinet's principle, the intensity distribution is

$$\begin{aligned} I &= [B \cdot \exp(i\phi_t) - b \cdot \exp(i\eta_t) + C \cdot \exp(\phi_r) - c \cdot \exp(i\eta_r)] \cdot [\text{c.c.}] \\ &= B^2 + C^2 + b^2 + c^2 - 2B \cdot b \cdot \cos(\phi_t - \eta_t) \\ &\quad - 2C \cdot c \cdot \cos(\phi_r - \eta_r) + 2b \cdot c \cdot \cos(\eta_t - \eta_r) \\ &\quad + 2B \cdot C \cdot \cos(\phi_t - \phi_r) - 2B \cdot c \cdot \cos(\phi_t - \eta_r) \\ &\quad - 2b \cdot C \cdot \cos(\eta_t - \phi_r). \end{aligned} \quad (23)$$

The first six terms are constants independent of the phase shift of the reference mirror. Since $2b \cdot c$ is so small that the seventh term, $2b \cdot c \cdot \cos(\eta_t - \eta_r)$, can be dropped, the intensity can be written as

$$I = 2B \cdot C \cdot \cos(\phi_t - \phi_r) - 2B \cdot c \cdot \cos(\phi_t - \eta_r) - 2b \cdot C \cdot \cos(\eta_t - \phi_r) + \text{constant}. \quad (24)$$

The first term in Eq. (24) determines the phase of interest; the second and third terms introduce phase error. Since both $\eta_r(x)$ and $\phi_r(x)$ vary according to the shifting of the reference mirror, the difference between $\eta_r(x)$ and $\phi_r(x)$ is independent of the shifting of the reference mirror, i.e., $\eta_r(x) = \phi_r(x) - \Delta(x)$. Therefore,

$$I_0 - I_2 = 4B \cdot C \cdot \cos(\phi_t - \phi_r) - 4B \cdot c \cdot \cos(\phi_t + \Delta - \phi_r) - 4b \cdot C \cdot \cos(\eta_t - \phi_r). \quad (25)$$

The corresponding maximum error is determined by the arccosine of the ratio $B \cdot c + b \cdot C$ to $B \cdot C$, when $\phi_t(x) + \Delta(x) - \eta_t(x)$ equals zero. In Fig. 6, around the point P the phase $\phi_t(x)$ does not vary as rapidly as the phases $\Delta(x)$ and $\eta_t(x)$. Since the phases $\Delta(x)$ and $\eta_t(x)$ are spherical wavefronts basically, the interference pattern and thus the residual phase error are circular.

References

1. J. H. Bruning, "Fringe Scanning Interferometers," in *Optical Shop Testing*, D. Malacara, Ed. (Wiley, New York, 1978), p. 409.

2. J. Schwider, R. Burow, K.-E. Elssner, J. Grzanna, R. Spolaczyk, and K. Merkel, "Digital Wave-front Measuring Interferometry: Some Systematic Error Sources," Appl. Opt. **22**, 3421 (1983).
3. J. C. Wyant, "Review of Phase Shifting Interferometry," in Technical Digest, *OSA Spring Meeting* (Optical Society of America, Washington, DC, 1984).
4. C. Ai and J. C. Wyant, "Effect of Piezoelectric Transducer Nonlinearity on Phase Shift Interferometry," Appl. Opt. **26**, 1112 (1987).
5. C. Ai, "Phase Measurement Accuracy Limitation in Phase Shifting Interferometry," Ph.D. Dissertation, U. Arizona, Tucson (1987).
6. J. C. Wyant, "Use of an ac Heterodyne Lateral Shear Interferometer with Real-time Wavefront Correction Systems," Appl. Opt. **14**, 2622 (1975).
7. P. Hariharan, "Digital Phase-Stepping Interferometry: Effects of Multiply Reflected Beams," Appl. Opt. **26**, 2506 (1987).

NASA *continued from page 3034*

This work was done by H. Douglas Garner, Anthony M. Busquets, Thomas W. Hogge, and Russell V. Parrish of Langley Research Center. This invention is owned by NASA, and a patent application has been filed. Inquiries concerning nonexclusive or exclusive license for its commercial development should be addressed to the Patent Counsel, Langley Research Center, G. F. Helfrich, Mail Code 279, Hampton, VA 23665. Refer to LAR-13626.

Wet-atmosphere generator

A portable flow-control system generates a nitrogen/water atmosphere having a range of dew points and pressures. One use of the system is to provide wet nitrogen for the canister of a wide-field camera that requires this special atmosphere. The system can also be used to inject trace gases other than water vapor for the leak testing of large vessels. Mixtures of gases can be used as carriers for the moisture. Potential applications are in photography, hospitals, and calibration laboratories.

The system uses pressurized nitrogen to power an ejector—essentially a Venturi tube with a line from a water-vapor supply tapped into the low-pressure region (see Fig. 10). The low pressure draws the vapor into the Venturi, where the vapor mixes with the main flow.

Liquid water for the vapor is held in a 3.8-liter (1-gal) bottle in the suitcaselike system housing. The line from the bottle to the ejector passes through a regulating valve that mechanically controls the flow by throttling. The pressure in the bottle is regulated by a heater; an operator sets the heater temperature to a value that yields a saturation pressure greater than the suction of the ejector.

Once mixed in the ejector, the water vapor and nitrogen are directed to an external vessel or to a vent by regulator valves. Valves may also be set to admit vacuum or return flow from the vessel to the system.

A sample line is tapped from the main flow line and sent to a dew-point sensor. The pressure at the sensor is regulated so that it is the same as that in the external vessel; this ensures an accurate reading because the dew point is a function of the pressure. If necessary, the operator adjusts the dew point by adjusting the flow of water vapor or nitrogen to the ejector.

The sensor is an automatically controlled optical device. A condensate-detector mirror is illuminated with an intense beam from a light-emitting diode. A photodetector monitors the light reflected from the mirror. The detector is fully illuminated when the mirror is clear but sees less light when dew forms on the mirror, scattering light out of the path to the detector.

The photodetector is part of a bridge circuit that produces a large output current when the mirror is dry. The bridge output is amplified and applied to a thermoelectric cooler, which reduces the temperature of the mirror. As dew begins to form on the mirror, the light to the photodetector starts to decrease, the bridge output current drops, and the thermoelectric cooling is reduced. A feedback loop in the sensor quickly stabilizes the thermoelectric cooling control so that a thin dew layer is maintained on the mirror. A precise thermometer embedded in the mirror monitors the dew-point temperature of the layer.

The sensor can reduce the temperature of the gas–vapor mixture by as much as 45°C. This means, for example, that, with the system at a temperature of 25°C, dew points between 25 and −20°C can be measured.

This work was done by Richard M. Hammer and Janice K. McGuire of Teledyne Brown Engineering Corp. for Marshall Space Flight Center. Inquiries concerning rights for the commercial use of this invention should be addressed to the Patent Counsel, L. D. Wofford, Jr., Mail Code CC01, Marshall Space Flight Center, AL 35812. Refer to MFS-28177.

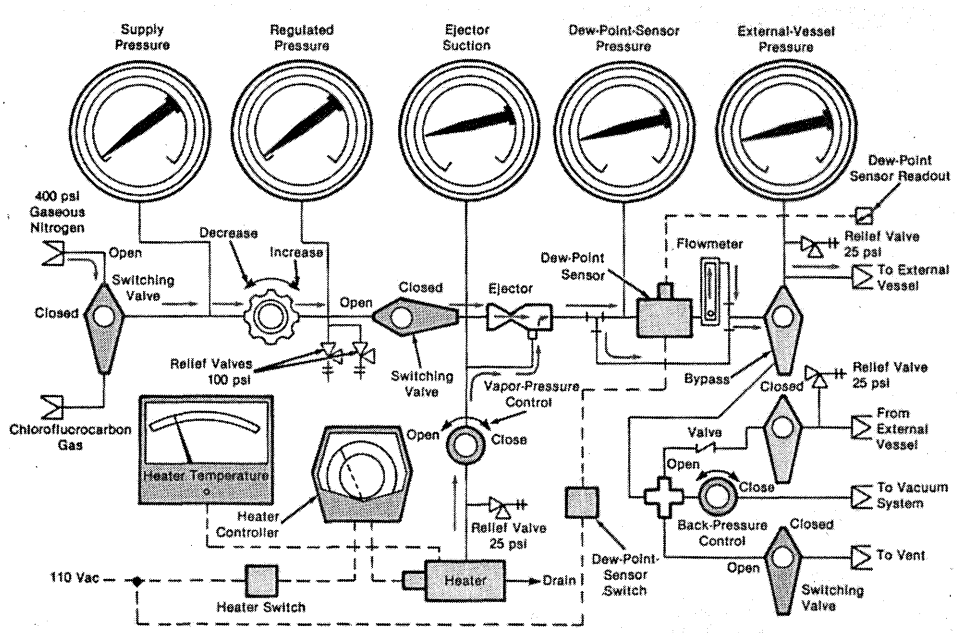

Fig. 10. Gas-flow conditions in the nitrogen, water vapor, and nitrogen–vapor mixture can be set by the operator with the help of these valves, gauges, and electrical controls.

continued on page 3050